Journal of Radiation Research and Applied Sciences 18 (2025) 101466

Contents lists available at ScienceDirect

Journal of Radiation Research and Applied Sciences

journal homepage: www.journals.elsevier.com/journal-of-radiation-research-and-applied-sciences

Comprehensive investigations of (Ti-6Al-4V - AA7075 / engine oil) nanofluid flowing with thermal radiative heat flux: Significant upshots

Syed M. Hussain [a], Misbah Arshad [b,*], Hijaz Ahmad [a,c,d], Wasim Jamshed [e,f,g,1], Kamel Guedri [h], Muhammad Amer Qureshi [i], Siti Suzilliana Putri Mohamed Isa [j,k], Abdulrazak H. Almaliki [l], Mustafa Bayram [m]

[a] Department of Mathematics, Faculty of Science, Islamic University of Madinah, Madinah, 42351, Saudi Arabia
[b] Department of Mathematics, COMSATS University Islamabad, Sahiwal Campus, Sahiwal, Pakistan
[c] Near East University, Operational Research Center in Healthcare, TRNC Mersin 10, Nicosia, 99138, Turkey
[d] Department of Mathematics, College of Science, Korea University, 145 Anam-ro, Seongbuk-gu, Seoul 02841, South Korea
[e] Department of Mathematics, Capital University of Science & Technology (CUST), 44000, Islamabad, Pakistan
[f] College of Engineering, Al-Ayen Iraqi University, An Nasiriyah, 64001, Iraq
[g] Department of Computer Engineering, Biruni University, Topkapi, Istanbul Turkey
[h] Mechanical Engineering Department, College of Engineering and Architecture, Umm Al-Qura University, P. O. Box 5555, Makkah, 21955, Saudi Arabia
[i] Department of Mathematical and Physical Sciences, College of Arts and Sciences, University of Nizwa, Nizwa, Sultanate of Oman
[j] Institute for Mathematical Research, Universiti Putra Malaysia, UPM Serdang, 43400, Selangor, Malaysia
[k] Centre for Foundation Studies in Science of Universiti Putra Malaysia, Universiti Putra Malaysia, UPM Serdang, 43400, Selangor, Malaysia
[l] Department of Civil Engineering, College of Engineering, Taif University, Taif, 21944, Saudi Arabia
[m] Department of Computer Engineering, Biruni University, 34010, Istanbul, Turkey

ARTICLE INFO

Keywords:
Thermal radiative heat flux
3rd-Grade nanofluids
Titanium & aluminum alloys
Symmetric extended surface
Variable thermal conductivity
Homotopy analysis method

ABSTRACT

A small number of researchers have investigated the fundamental nature of nanomaterials, specifically regarding the symmetrical elongated surface effectiveness of third-grade nano-liquids (3-GNF). In this article, motor oil is selected as the common base fluid for the 3-GNF version. This decision was inspired by the Tiwari and Das fluid model. Tiwari and Das examined the percentage of nanoparticles in the Buongiorno model, considering thermophoresis and Brownian diffusion variables. Because of this, the thermal performance of 3-GNF is investigated in the study that is now being written. Because of this, the conceptual model utilizes symmetry in its description. To generate nonlinear ordinary differential equations, it is necessary to first use the transformation method to partial differential equations that are generated using the boundary-layer formulation. The final numerical solutions are then obtained by using the homotopy evaluation technique in Mathematica, which is a part of the semi-analytical machine. It is taken into consideration that titanium alloys (Ti-6Al-4V) and aluminum alloys (AA7075) also exist. There is a significant difference in the thermal performance of the Ti-6Al-4V-EO nanofluid and that of the AA7075-EO nanofluid, as determined by the numerical results that were done in the same condition. Moreover, the thermal Biot number increases temperature while variable thermal conductivity decreases it. Further, the spongy medium reduces the thermal source charge and enhances rate variation. Finally, the effect of Reynolds and Brinkman numbers is increasing entropy. The present framework is beneficial in the medicinal and commercial domains, especially in the areas of biomedical cooling technologies, drug delivery, and the treatment of hyperthermia.

1. Introduction

Boundary flow is important especially in fluid regions and areas with significant wall collision influence. The initial assumption states that the fluid in the vicinity of the plate cannot flow. However, the fluid in this location has the same rate of movement as the plate. In addition, the

This article is part of a special issue entitled: Radiation Sciences and Applications published in Journal of Radiation Research and Applied Sciences.

* Corresponding author.
E-mail address: misbaharshad90@yahoo.com (M. Arshad).

[1] Distinguished Scientist in Top 2 % of Scientists by Stanford University list (2022, 2023 & 2024).

https://doi.org/10.1016/j.jrras.2025.101466
Received 11 March 2025; Received in revised form 21 March 2025; Accepted 23 March 2025
Available online 7 April 2025
1687-8507/© 2025 The Authors. Published by Elsevier B.V. on behalf of The Egyptian Society of Radiation Sciences and Applications. This is an open access article under the CC BY-NC-ND license (http://creativecommons.org/licenses/by-nc-nd/4.0/).

flow regions stimulated through the prevailing stress gradient are no longer under interest (Davey, 1961). In 1904, Ludwig Prandtl suggested the concept of a boundary layer, which introduced the theory of pores and skin tension, wall heat transfer, and boundary separation. The boundary layer theory can be applied to the movement of planes, transports, and various automobiles. Subsequently, the Prandtl proposal has been described in detail (Tulapurkara, 2005). The fluid boundary layer is fluid in the region of the binding location, where the viscosity effect is significant. In fluid mechanics, a skinny layer of flowing fuel line or fluid touches a place similar to the wing of a plane or the interior of a pipe. The shear strength is applied to the liquid only within the boundary layer. So long as the liquid hits the floor, the rate varies across the boundary layer from peak to zero. The application of the boundary layer theory on the plane has been reported as follows: The boundary layers on the plane's wing are thin at the front margins and border on the back margins (Epifanov, 2011). The boundary layer is proven to influence the flow by controlling flow parameters, including velocity and stress reduction (Benetti et al., 2015). The applications of the cross-border flow have been reported by controlling the flow characteristics. One of the examples is the movement of airfoil (Sullerey et al., 2002). Meanwhile, the idea of a boundary layer shows that the glide of Reynolds excessive numbers may be divided into major inequalities regions. At the highest flow rate in a fluid boundary layer, the viscosity in a fluid boundary layer may be ignored. However, the viscosity should be considered at the thinnest boundary of the wall (Schlichting & Gersten, 2016).

Many engineering methods in the packaging industry rely on the flow over a stretched surface. One of the applications is the production of polymer. Polymer sheets are manufactured in the industry by continuously extruding polymer from a die to a windup roller placed a finite distance away. The polymer sheet is produced when the thin layer of polymer is extended non-uniformly at ambient fluid (Takhar et al., 2001). Besides, the stretching rate is observed to be proportional to the length measured from the origin point (Vleggaar, 1977). The pioneer researcher in this scope of study is Crane, where he is successfully solved the Navier–Stokes equations for the two-dimensional fluid model bounded by a stretching sheet (Crane, 1970). Subsequently, a large body of research has been published in this area (Abraham & Sparrow, 2005; Andersson et al., 1992; Lakshmisha et al., 1988; Magyari & Keller, 2000; Sparrow & Abraham, 2005; Wang, 1984).

A nanofluid is a liquid containing nanometer-sized particles known as nanomaterials. The most selected nanomaterials are metals, oxides, carbides, or nano-tubes. Water is extensively employed as an active liquid due to its widespread availability. However, water is not the top selection because it has low thermal conductivity. Other options for active liquid instead of water are engine oil, ethylene glycol, and other non-exchange fluids. However, these chemicals' highly viscid and hazardous environment limits their employment in heat transfer procedures (Pozhar, 2000). The nanofluid with a liquid, which has a combination of ethylene glycol and water improves the engine cooling rate because this combination acts as a car coolant. In recent years, electronics conditioning of silicon chips and microcomputer circuits with the involvement of nanofluids has evolved. (Rafati et al., 2012). Aluminum and titanium alloys are used in the present work due to their notable strength-to-weight ratio, capability to resist corrosion, and thermal endurance, which make them fundamental for use in biomedicinal, automobiles, and aerospace industries. When used in high-performance engineering systems, these alloys improve structural efficiency. They are significant to industry because they boost modern production techniques, durability, and energy efficiency. As a conclusion, nanofluid is proven to play an important role in heat transfer behaviour, compared to the conventional fluid (Polidori et al., 2007). Recent research (Jawad et al., 2024a, 2024b; Ramasekhar et al., 2024; Ramasekhar & Jawad, 2024; Waseem et al., 2025) has examined the sophisticated heat transfer properties of nanofluids, emphasizing their improved stability, efficiency, and thermal conductivity in industrial and biomedical applications. These investigations offer important new information about how nanoparticles can enhance convective heat transfer and maximize thermal control systems.

The relevant studies of third-grade fluids have being reported, based on these scope: due to the specific type of non-Newtonian fluid (Rivlin & Ericksen, 1997), influenced by Soret-Dufour effects (Hayat et al., 2012), over the two stretchable rotating disks (Turkyilmazoglu, 2016), subjected to the viscous dissipation and Newtonian heating (Shehzad et al., 2015), over a permeable surface with partial slip (Sajid et al., 2008), the flow configurations among two equal surfaces (Rashidi et al., 2008), based on the Cattaneo-Christov heat flux model (Shehzad et al., 2016), three-layered rotating outline (Hussnain et al., 2012), with the existence of stagnation point (Baris, 2003), with the effect of suction (Shoaib et al., 2016), mixed convection (Ramzan et al., 2016), convective conditions (Mustafa et al., 2014), containing gyrotactic microorganisms (Alzahrani et al., 2019), (McKee, 2024), thermodynamics and steadiness theory of the third-grade fluids (Fosdick & Rajagopal, 1980), the pipe flow (Yürüsoy & Pakdemirli, 2002), temperature dependent thermophysical characteristics (Sohail et al., 2019), four-phase fluid (Yuan et al., 2024), quadratic thermal radiation in a disk (Sohail et al., 2024), MHD flow with various viscosity (Ellahi & Riaz, 2010), over a vertical channel (Adesanya & Makinde, 2015), axisymmetric squeezing flow (Hayat et al., 2017), exponential curved sheet (Anantha Kumar et al., 2020), over a porous channel (Akinshilo & Sobamowo, 2017), unsteady state of flow (Reddy et al., 2018), MHD flow over a cone (Gaffar et al., 2018), over a blade coating (Sajid et al., 2019), and with Brownian motion and thermophoresis effects (Mahanthesh & Joseph, 2019). As of late nanofluid streams with warm conduct under the impacts of attractive powers in various calculations were reviewed by Shah et al. (Shah, Babazadeh, et al., 2019), (Shah, Kumam, et al., 2019).

The homotopy analysis technique (HAM) is a powerful mathematical tool for solving computational complexity. The use of HAM to reveal the convergence of the collected solution is unusual in analytic and semi-analytic approaches for nonlinear partial differential equations (Liao, 2004). Liao (Liao, 1992) provided a realistic analytic method for complex equations, namely the homotopy evaluation method (Liao, 1999a, 1999b). Moreover, the benefit of HAM is it can obtain an accurate estimation for a nonlinear problem by determining individual units of base functions (Liao & Cheung, 2003).

Recently, a few researchers have explored entropy age in the progression of liquids and hotness moving over an extending surface. The display of heating and cooling is vital in many electrical and energy difficulties in various design and current divisions. Aiboud and Saouli (Aïboud & Saouli, 2010) used entropy exploration and Kummer's aptitude to analyze the MHD viscoelastic liquid cascade. Makinde (Makinde, 2011) calculated the entropy age number via shooting quadrature by including the heated radiation and Newtonian heating influences of variable constancy liquid. Loganathan et al. (Loganathan et al., 2021), (Loganathan & Rajan, 2020) investigated the entropy examination for the third-grade and Williamson nano-liquid stream. The entropy applications have being discovered in scientific and materials engineering, cosmological, environmental sciences, ecological degradation, etc (Naz et al., 2020; Torres-Mendieta et al., 2016).

Concerning the execution of managing parameters such as porous materials, variability thermal conducting, radioactivity heating flux, and slippage conditions, neither of the specific investigations that were noted considered the Tiwari-Das nano liquid framework throughout the extensible sheet. This is following the findings of the previous studies. Because of this, the current investigation focuses on the regulating parameters and entropy that were discussed before by using a one-of-a-kind semi-numerical approach known as the homotopy analysis method.

2. Mathematical formulation

The velocity $U_w(x,0)$ and the temperature $¥_w(x,0)$ at the wall (fixed at $x = 0$) are formulated as (Alkathiri et al., 2022):

$$U_w(x,0)=bx, ¥_w(x,0)=¥_\infty+b^* x, \tag{2.1}$$

Here b is an original expanding rate. $¥_w(x,0)=¥_\infty+b^* x$, signifies insulated wall temperature. Here b^*, $¥_w$ and $¥_\infty$ signify the rate of temperature difference, the temperature of the wall and surrounds, correspondingly. The dimension of 3-GNF flow is depicted in Fig. 1

The requirements of the stream framework in this paper are.

2-D laminar steady flow,
3^{rd} GNF,
variable thermal conductivity,
phase flow model,
permeable medium,
porousness elongated surface.

The constitutive relations of flowing around a nasty 3rd-grade nanofluid using standard boundary layer assumptions, porousness media, varying thermal conducting, and radiative heat fluxing are (Ali et al., 2022):

$$u_x+v_y=0, \tag{2.2}$$

$$uu_x+vu_y=\frac{\mu_{nf}}{\rho_{nf}}u_{yy}+\frac{\lambda_1}{\rho_{nf}}(uu_{xyy}+3u_yu_{xy}+u_xu_{yy}+vu_{yyy})+\frac{2\lambda_2}{\rho_{nf}}(u_yu_{xy}) +\frac{6\lambda_3}{\rho_{nf}}(u_y)^2u_{yy}-\frac{\mu_{nf}}{\rho_{nf}}\frac{u}{k}, \tag{2.3}$$

$$uT_x+vT_y=\frac{1}{(\rho C_p)_{nf}}\left[\frac{\partial}{\partial y}\left(\kappa^*_{nf}(T)T_y\right)\right]-\frac{1}{(\rho C_p)_{nf}}(q_r)_y. \tag{2.4}$$

The related boundary constraints are

$$\left.\begin{array}{c} u(x,0)=U_w+N_L(u_y), v(x,0)=V_w, -k_0(T_y)=h_f(T_w-T), \\ u\to 0, \frac{\partial u}{\partial y}\to 0, T\to T_\infty \quad as \quad y\to\infty. \end{array}\right\} \tag{2.5}$$

Where,

flow velocity ($\overleftarrow{V}=[u(x,y), v(x,y), 0]$),
variable thermal conductivity ($\kappa^*_{nf}(T)$),
slip length (N_L),
surface permeability (V_w),
temperature (¥),
porosity (k),
heat transport factor (h_f),
thermal conducting of surface (k_O).

The nanomaterials dispersal in aqueous fluid results shown in increased thermal-physical properties. The properties of the material for 3-GNF are listed in Table 1.

ϕ is the nanoparticle volumetric fraction coefficient, $\rho_f, \mu_f, \sigma_f, \kappa_f$ and $(C_p)_f$ are consistency, dynamic viscidness, electrical conducting, thermal conducting, and adequate heat capacity of the normal liquid individually.

The additional properties ρ_s, σ_s, κ_s, $(C_p)_s$ are the consistency, electrical and thermal conductance's adequate heat capacity of the nano molecules, correspondingly. The variable thermal conducting is defined as (Jamshed & Aziz, 2018):

$$\kappa^*_{nf}(T)=k_{nf}\left[1+\epsilon(T-T_\infty)(T_w-T_\infty)^{-1}\right] \tag{2.6}$$

Table 2 displays the substantial properties of the standard liquid locomotive oil and the various nano molecules used in this study,

Utilizing the Roseland guesstimate, we get

$$q_r=-1.33\frac{\sigma^*}{k^*}(T^4)_y, \tag{2.7}$$

Here, σ^* is the Stefan Boltzmann number and k^* is the absorption coefficient.

3. Problem solution

The (BVP) equations (2.1)-(2.4) are converted using the similarity approach, which turns the controlling PDEs into ODEs. The introduction of streaming function ψ of the type

$$u=\psi_y, v=-\psi_x. \tag{3.1}$$

and similarity conversions of the way

$$\eta(x,y)=\sqrt{\frac{b}{\nu_f}}y, \psi(x,y)=\sqrt{\nu_f b}xf(\eta), \theta(\eta)=(T-T_\infty)(T_w-T_\infty)^{-1}. \tag{3.2}$$

into equations (2.1)-(2.4). We get

$$f'''+\phi_1\left[\phi_2(ff''-f'^2)+B_1\left(2f'f'''-ff^{iv}\right)+3(B_1+B_2)f''^2 +6B_3R_ef''^2f'''-\frac{1}{\phi 1}Kf'\right]=0, \tag{3.3}$$

$$\theta''\left(1+\epsilon\theta+\frac{1}{\phi_4}P_rN_r\right)+\epsilon\theta'^2+Pr\frac{\phi_3}{\phi_4}(f\theta'-f\theta)=0, \tag{3.4}$$

with

$$\left.\begin{array}{l} f(0)=S, f'(0)=1+\Lambda f''(0), \theta'(0)=-B_\varsigma(1-\theta(0)) \\ f'(\eta)\to 0, f''(\eta)\to 0, \theta(\eta)\to 0, as \quad \eta\to\infty \end{array}\right\}. \tag{3.5}$$

here $\phi_i's$; $1\le i\le 4$ for the inequalities (3.3)–(3.4) represent the following physical thermal assets for the third-grade nanoliquid

$$\left.\begin{array}{l} \phi_1=(1-\phi)^{2.5}, \phi_2=\left(1-\phi+\phi\frac{\rho_s}{\rho_f}\right), \phi_3=\left(1-\phi+\phi\frac{(\rho C_p)_s}{(\rho C_p)_f}\right), \\ \phi_4=\left(\frac{(k_s+2k_f)-2\phi(k_f-k_s)}{(k_s+2k_f)+\phi(k_f-k_s)}\right). \end{array}\right\} \tag{3.6}$$

It is remarked that equality (2.1) is identically contented. In the beyond

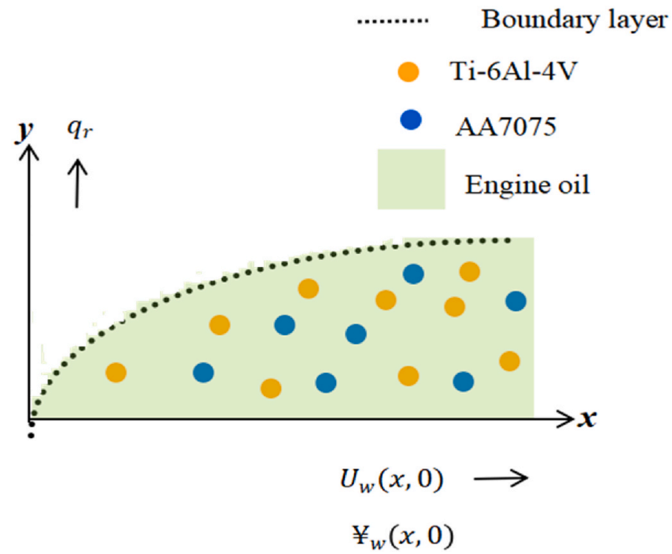

Fig. 1. Flow model figure.

equalities, ' takes derivatives concerning ϖ. $B_1 = \frac{b\lambda_1}{\mu_f}$, $B_2 = \frac{b\lambda_2}{\mu_f}$ and $B_3 = \frac{b\lambda_3}{\mu_f}$ indicates the material parameters for third-grade fluid and $= \frac{\nu_f}{b\kappa_f}$, respectively. $P_r = \frac{\nu_f}{\alpha_f}$ represent the Prandtl quantity. Thermal diffusion factor, warmth cause, transference of mass, and radiative's warmth parameters are provided by $\alpha_f = \frac{\kappa_f}{(\rho C_p)_f}$, $S = -V_w\sqrt{\frac{1}{\nu_f b}}$ and $N_r = \frac{16}{3}\frac{\sigma^* T_\infty^3}{\kappa^* \nu_f (\rho C_p)_f}$ respectively. $\Lambda = \sqrt{\frac{b}{\nu_f}} N_L$ is the rapidity slippage factor. $R_e = \frac{bx^2}{\nu_f}$ and $B_\varsigma = \frac{h_f}{k_0}\sqrt{\frac{\nu_f}{b}}$ are Reynolds and Biot numbers, respectively. The local Nusselt quantity (Nu_x) is the physical quantity of importance that regulate the radiance and can be confirmed as (Ali et al., 2022)

$$Nu_x = \frac{xq_w}{k_f(T_w - T_\infty)} \tag{3.7}$$

wherein q_w embodies the heat fluxing defined by

$$q_w = -k_{nf}\left(1 + 5.33\frac{\sigma^* T_\infty^3}{\kappa^* \nu_f (\rho C_p)_f}\right)((T_y))_{y=0} \tag{3.8}$$

Using the dimensionless adjustments (3.2), we get

$$Nu_x Re_x^{-\frac{1}{2}} = -\frac{k_{nf}}{k_f}(1 + N_r)\theta'(0), \tag{3.9}$$

where Nu_x signifies Nusselt quantity and C_f implies the reduced frictional force. $Re_x = \frac{U_w x}{\nu_f}$ is local Re differs from the stretchable rapidity $(U_w(x))$.

4. Entropy generating simulation

The entropy generated for the suppositions, as revealed above, is (Shahzad et al., 2021):

Table 1
The primary properties of nanofluid (Jamshed et al., 2021).

Properties	Nanofluids
Dynamic Viscidness	$\mu_{nf} = \mu_f(1-\phi)^{-2.5}$
Consistency	$\rho_{nf} = (1-\phi)\rho_f + \phi\rho_s$
Heat Capacitance	$(\rho C_p)_{nf} = (1-\phi)(\rho C_p)_f + \phi(\rho C_p)_s$
Thermal Conducting	$\frac{k_{nf}}{k_f} = \left[\frac{(k_s + 2k_f) - 2\phi(k_f - k_s)}{(k_s + 2k_f) + \phi(k_f - k_s)}\right]$

$$E_G = \frac{k_{nf}}{T_\infty^2}\left\{(T_y)^2\left(1 + 5.33\frac{\sigma^* T_\infty^3}{\kappa^* \nu_f (\rho C_p)_f}\right)\right\} + \frac{\mu_{nf}}{T_\infty}((u_y))^2 + \frac{\mu_{nf} u^2}{kT_\infty}. \tag{3.10}$$

The dimensionless form of entropy equality is obtained as

$$N_G = \frac{{T_\infty}^2 b^2 E_G}{k_f(T_w - T_\infty)^2}. \tag{3.11}$$

From equality (3.2), the nondimensional entropy relation is:

$$NG = Re\phi 4(1+Nr)\theta'2 + 1\phi 1\mathrm{Br}\Omega f''2 + Kf'2.\ N_G = R_e\left[\phi_4(1+N_r)\theta'^2 + \frac{1}{\phi_1}\frac{B_r}{\Omega}\left(f''^2 + Kf'^2\right)\right]. \tag{3.12}$$

5. Homotopy analysis method

Liao presented the homotopy method in 1992. In contemplation of acquiring the solutions of nonlinear models, the homotopic technique is advantageous. In Fig. 2, the homotopy approach includes the following steps:

Further, it gives a lot of flexibility to choose the initial guesses as well as linear operators, which are written as follows:

$$\left.\begin{aligned} f(\varpi) &= S + \frac{1}{1+\Lambda}(1 - e^{-\varpi}), \\ \theta(\varpi) &= \frac{B_c}{1+B_c}(e^{-\varpi}), \\ L_f(f) &= \frac{d^3 f}{d\varpi^3} - \frac{df}{d\varpi}, L_\theta(\theta) = \frac{d^2\theta}{d\varpi^2} - \theta. \end{aligned}\right\} \tag{4.1}$$

With

$$\left.\begin{aligned} L_f[A_1 + A_2 e^{-\varpi} + A_3 e^{\varpi}] = 0, \\ L_\theta = [A_4 e^{-\varpi} + A_5 e^{\varpi}] = 0. \end{aligned}\right\} \tag{4.2}$$

here $A_i (i = 1, 2, ..., 5)$ signify the optional fixed values.

The general solutions (f_m, θ_m) are represented by

$$\left.\begin{aligned} f_m(\varpi) &= f_m^*(\varpi) + A_1 + A_2 e^{-\varpi} + A_3 e^{\varpi}, \\ \theta_m(\varpi) &= \theta_m^*(\varpi) + A_4 e^{-\varpi} + A_5 e^{\varpi}. \end{aligned}\right\} \tag{4.3}$$

Here $f_m^*(\varpi)$ and $\theta_m^*(\varpi)$ demonstrate unique solutions.

6. Code genuineness

The verification of the numerical technique was performed by comparing the outcomes of the heat transmission rate from the previous works (Abu-Hamdeh et al., 2021; Makinde & Aziz, 2011), which are tabulated in Table 3.

7. Graphical results and discussion

Third-grade liquids are a subcategory of non-Newtonianism liquids that include non-Newtonianism phenomena such as shear thinning, thickening, and normal stresses, even in rigid boundaries. Additionally, it possesses viscid elastic fluid properties. The physical parameters outcome is using AA7075 -EO and Ti-6Al-4V –EO, the non-Newtonian 3-GNF.

Table 2
The primary estates of the normal liquid and nano molecules at a standard temperature (Adnan et al., 2021; Iqbal et al., 2021; Makinde et al., 2018).

Thermophysical Properties	$\rho(kg/m^3)$	$c_p(J/kgK)$	$k(W/mK)$
Ti-6Al-4V (titanium alloy)	4420	0.56	7.2
Engine Oil (EO)	884	1910	0.144
AA7075 (aluminium alloy)	2810	960	173

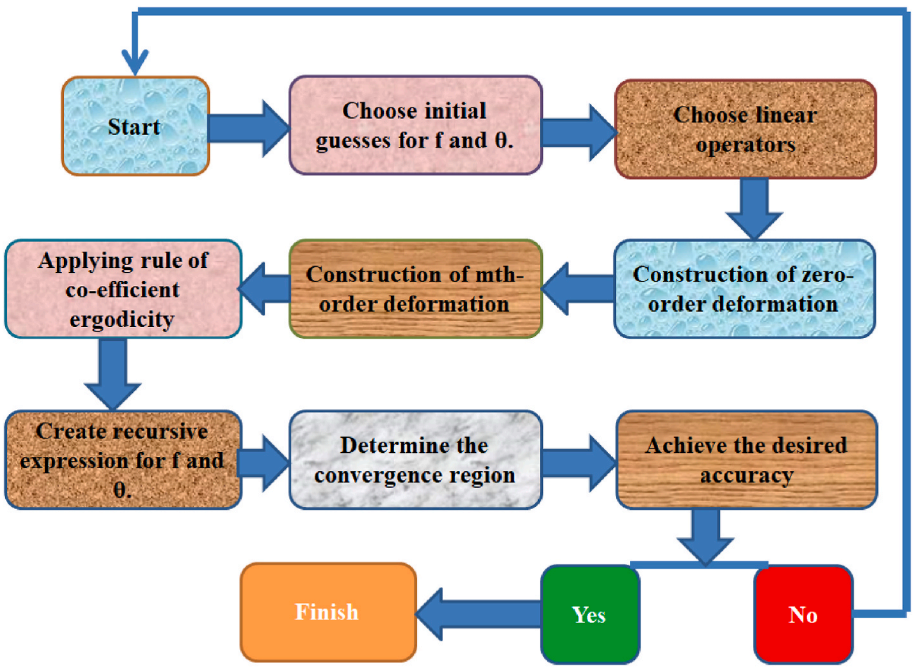

Fig. 2. Flow chart.

Table 3
Comparing values of heat transmission rate $-\theta'(0)$ for various Prandtl numbers, when $\epsilon = 0$, $\phi = 0$, $\Lambda = 0$, $S = 0$ and $B_\varsigma \to \infty$.

P_r	Ref. (Makinde & Aziz, 2011)	Ref. (Abu-Hamdeh et al., 2021)	Present
0.72	0.1691	0.1690	0.1690
1.0	0.4539	0.4537	0.4537
3.0	0.9114	0.9113	0.9113
7.0	1.8954	1.8958	1.8958

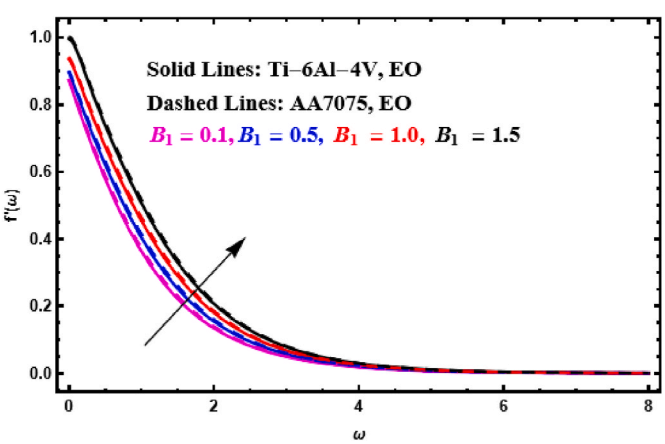

Fig. 3(a). Velocity variation versus B_1.

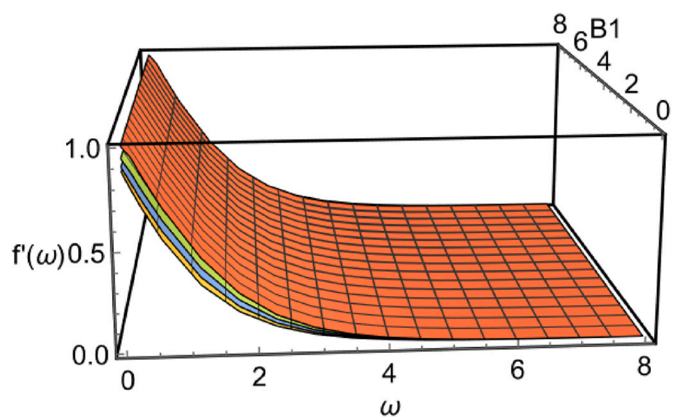

Fig. 3(b). Velocity variation versus B_1.

7.1. Velocity profiles

It is critical to analyze the behaviour of the velocity profile with the existence of governing physical parameters, as described below.

7.1.1. Impact of the material parameters for third-grade fluid

When different values of B_1 were used to depict the behaviour of both nanofluids; the result is shown in Fig. 3(a). The flow velocity of both types of nanofluids is amplified as a result of the enhancement of B_1. This result is attributable to the fact that the basis fluid is easily

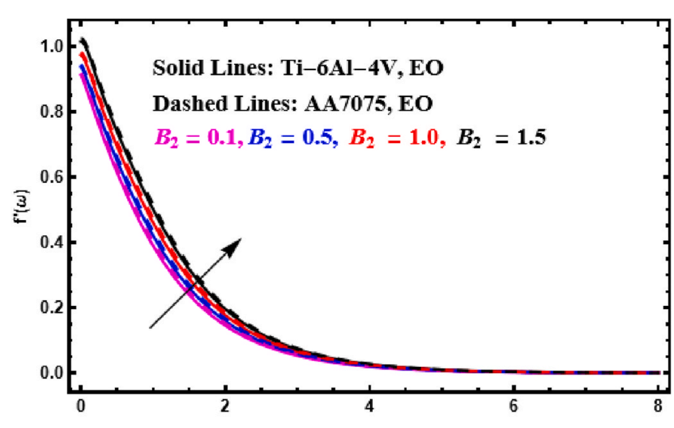

Fig. 4(a). Velocity variation versus B_2.

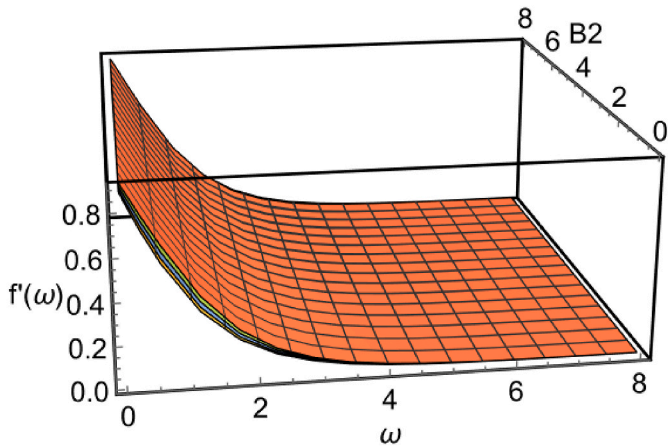

Fig. 4(b). Velocity variation versus B_2.

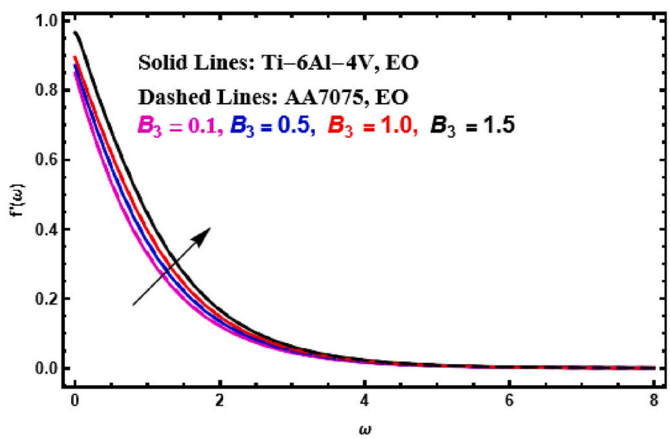

Fig. 5(a). Velocity variation versus B_3.

changed by B_1, which is a significant component. By careful examination, it has been discovered that AA7075-EO has a greater velocity than Ti-6Al-4V-EO. As a result of this fact, the thickness of the Ti-6Al-4V-EO's momentum boundary layer will be augmented. The velocity profile in 3-D is illustrated in Fig. 3(b) for a clearer view of changing the value of B_1. The increment of velocity is evenly distributed along with the flow as B_1 enhanced.

While the third-grade parameter B_2 is strengthened, Fig. 4(a) depicts the velocity distribution. This phrase indicates that the fluid velocity has increased significantly. This process results in a dilatation of the momentum boundary layer's breadth. Nonetheless, Ti-6Al-4V-EO has considerably faster acceleration than AA7075-EO. Viscosity does not appear to affect Ti-6Al-4V-EO in this circumstance significantly. The fluid width can be declined by modifying the well-known third-grade parameter. Fig. 4(b) illustrates the velocity profile in three dimensions to help see the changing value of B_2. As B_2 is strengthened, the velocity increment is distributed equally along with the flow.

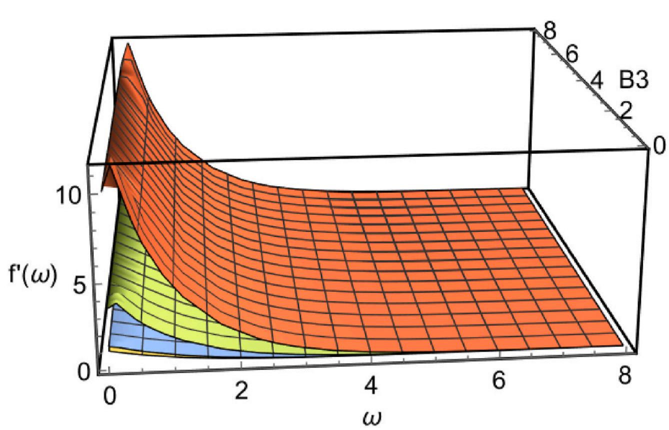

Fig. 5(b). Velocity variation versus B_3.

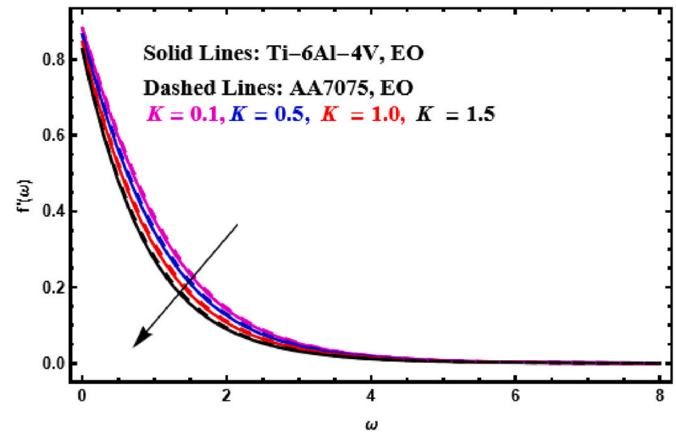

Fig. 6(a). Velocity variation againts K.

Conversely, as the third-grade parameter B_3 grows, the velocity surges as well, as demonstrated in Fig. 5(a). It shows that AA7075-EO had a higher speed than Ti-6Al-4V-EO. The decrement of the fluid boundary thickness is shown, when Ti-6Al-4V-EO is used as a nanofluid. This phenomenon is acceptable since AA7075-EO has a minor influence on the third-grade metric B_3. Meanwhile, Fig. 5(b) shows that the velocity profile changes in three dimensions, making it easier to discern when B_3 changes. The velocity increase is evenly spread over the flow when B_3 is reinforced.

7.1.2. *Impact of porousness material parameter* (K)

To state of the art, it was offsetting the intensities from the empty percentage yields the permeability of a substance K. Porosity, as well recognized, influences the structure's measurement of skin friction. Fig. 6(a) demonstrates the critical role of porosity around the velocity profile for both types of nanofluids. Both fluids demonstrated the characteristics described above in terms of porosity growth. The acceleration in velocity is a result of K being pruned. These conditions exist since the friction between the flow, and the surface is an exclave, causing the velocity to shrink. Improving porosity should be employed to minimize resistance between the nanofluid particles and the outer plate.

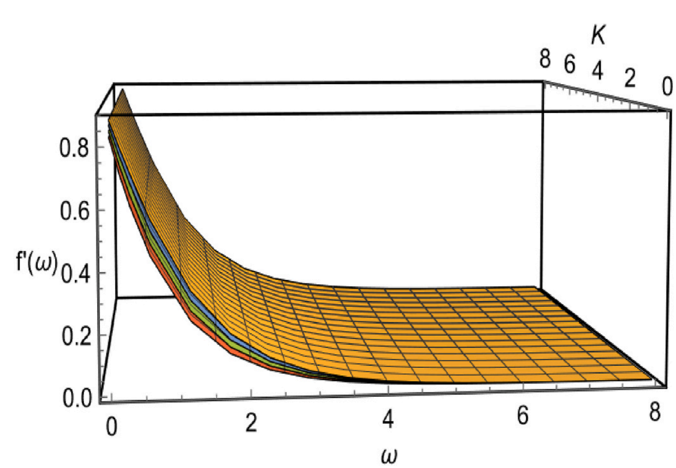

Fig. 6(b). Velocity variation againts K.

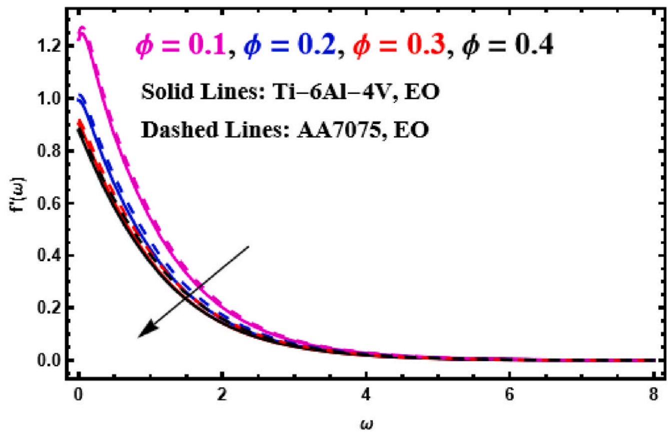

Fig. 7(a). Velocity variation against ϕ.

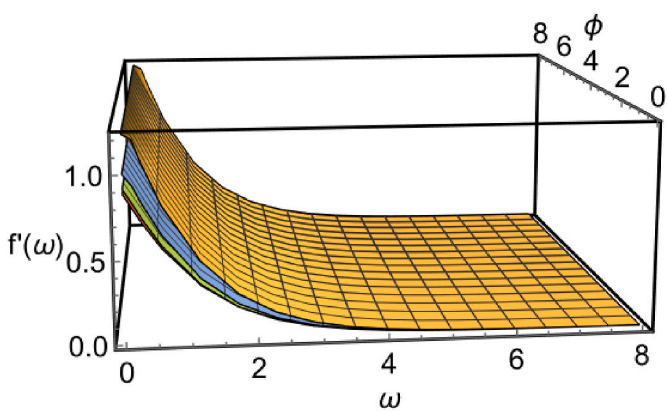

Fig. 7(b). Velocity variation against ϕ.

It's worth noting that while Ti-6Al-4V-EO flows more sluggish than other nanofluids, its impetus boundary thickener is more refined than that of AA7075-EO. As the porosity of the material upsurges, surprisingly, Ti-6Al-4V-EO and AA7075-EO cooperatively boosted the temperature profile. With a lower porous medium parameter value, there will be more heat relegation. K are visible in Fig. 6(b) because the velocity profile changes in three dimensions. It was strengthening K, resulting in a uniform distribution of diminished flow velocity.

7.1.3. The effect of the nanoparticle volume fraction parameter (ϕ)

The solvent volume of the nanofluid is equivalent to the total of its components' volumes. A metal nanoparticle's volume fraction is computed before calculating the total mixture, by apportioning the mixture's volume by the component's volume. Fig. 7(a) shows that nanoparticle volume fraction affects particle velocity. Growing the volume percentage of nanoparticles in both nanofluids reduces the fluid dynamics speed. The collective fluid viscosity that results from the accumulation of nanofluid concentration and the widening of the friction is the cause of this phenomenon. Compared to the Ti-6Al-4V-EO nanofluid, the AA7075-EO nanofluid has a much higher velocity due to the enhancement. In Fig. 7(b), the velocity profile changes in three dimensions, making ϕ evident. When ϕ is amplified, the flow velocity diminutions in a uniform manner.

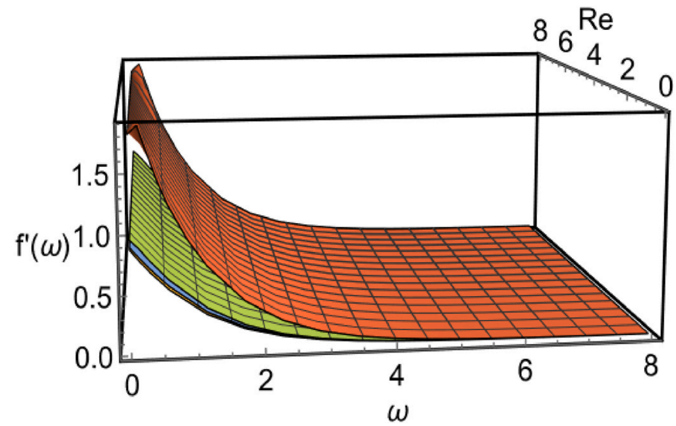

Fig. 8(b). Velocity variation versus R_e.

7.1.4. Impact of Reynolds number (R_e)

Inertial forces improve the system's velocity, as seen in Fig. 8(a), leading to a rise in the Reynold number. The movement rate of nanoparticles is increased with the higher kinetic energy, proved by the enhancing Reynolds number. As a result, the velocity of the Ti-6Al-4V-EO nanofluid it's astonishingly lower than AA7075-EO. Compared to AA7075, Ti-6Al-4V has a significantly stronger affinity for base fluids. This phenomenon means that a smaller Reynolds number can't quickly destabilize the system as it could otherwise. Fig. 8(b) shows a three-dimensional variation in the velocity profile, which demonstrates the existence of R_e. Flow velocity decreases uniformly when R_e is increased.

7.1.5. Impact of suction ($S > 0$) parameter

Flow effects of various suction settings must be considered. As seen in Fig. 9(a), as suction increases, flow velocity decreases. The suction action will disrupt the surface flow. As a result, over time, the flow

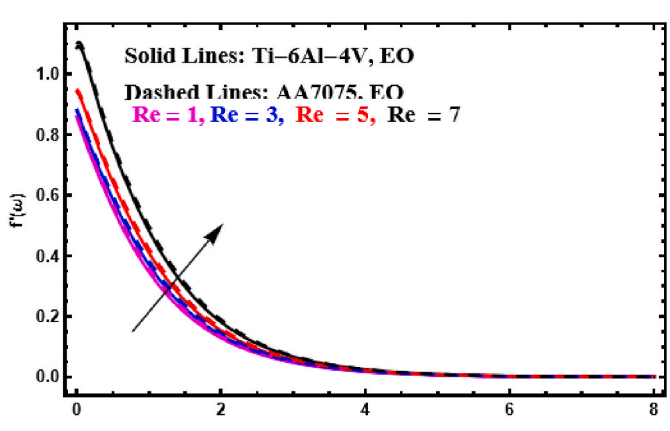

Fig. 8(a). Velocity variation versus R_e.

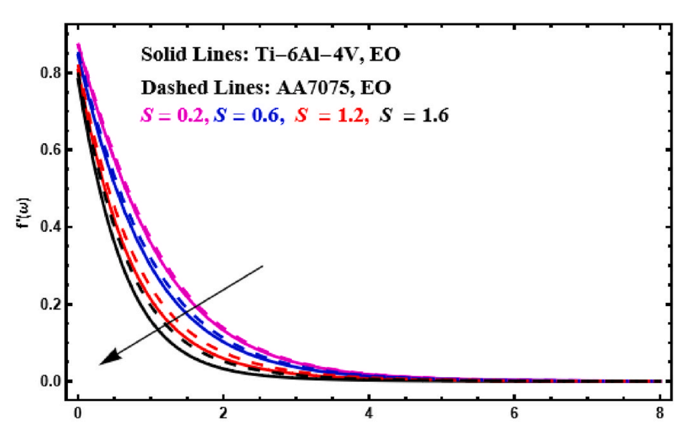

Fig. 9(a). Velocity variation against S.

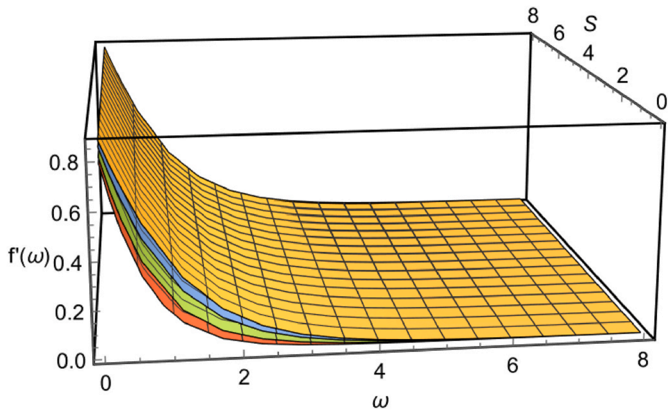

Fig. 9(b). Velocity variation against S. 7.1.6 Impact of velocity slip parameter (Λ).

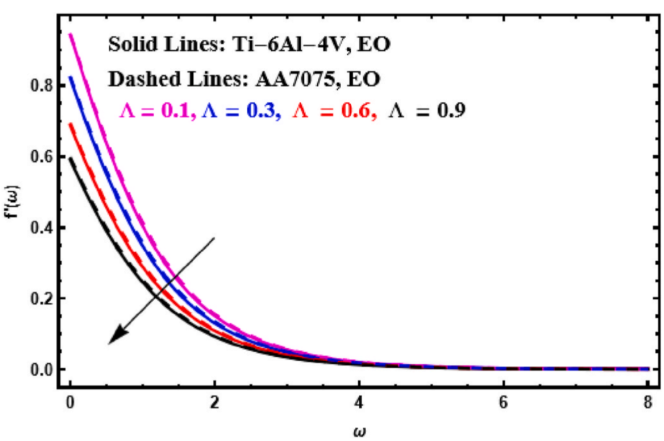

Fig. 10(a). Velocity variation against Λ.

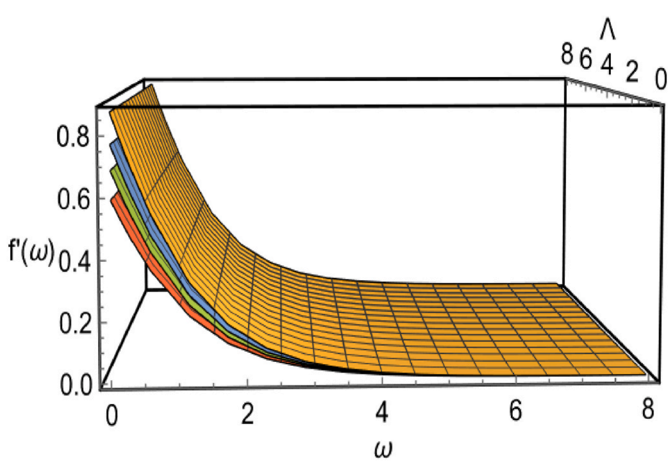

Fig. 10(b). Velocity variation against Λ. 7.2 Temperature Profiles.

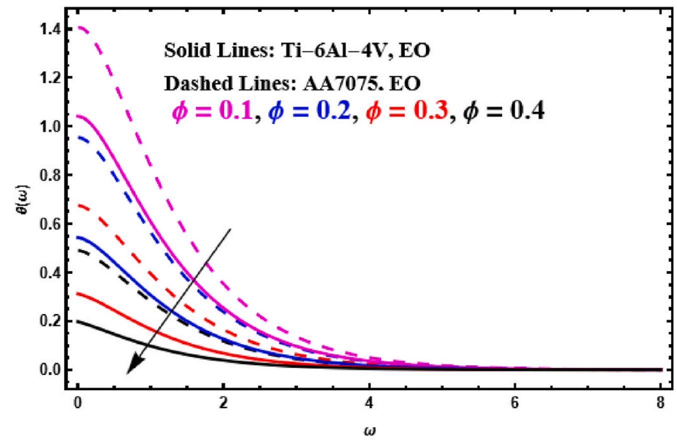

Fig. 11(a). Temperature variation against ϕ.

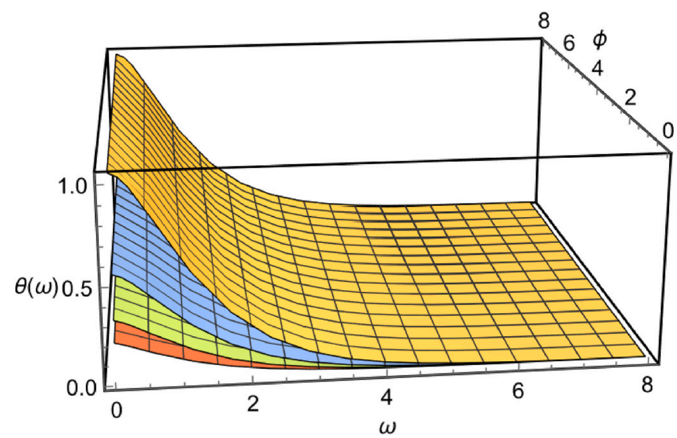

Fig. 11(b). Temperature variation against ϕ. 7.2.2 Impact of Biot number ($\boldsymbol{B_\varsigma}$).

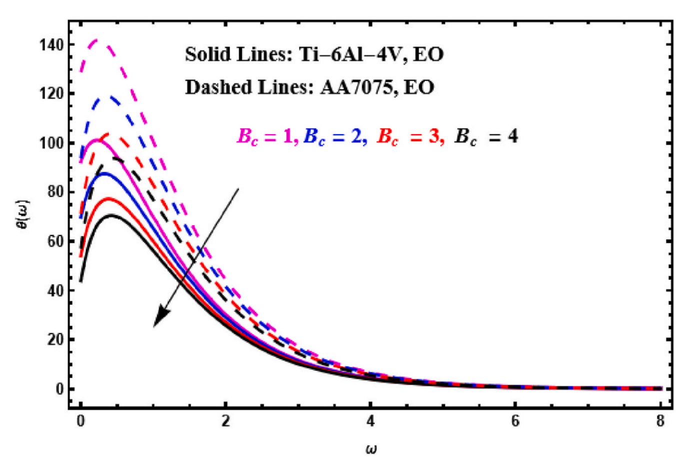

Fig. 12(a). Temperature variation versus B_ς.

velocity will cause shrinkage. The AA7075-EO seemed to have slowed down at the outset. The molecule of AA7075-EO is considerably smaller than the molecule of Ti-6Al-4V-EO; it is simpler for AA7075-EO to travel about by the pull force of the arrangement. As can be seen in Fig. 9(b), the velocity profile exhibits a three-dimensional fluctuation that proves the existence of suction. When suction is raised, uniform flow velocity drops.

The velocity differential between the airborne particles and the expelled particle is specified by the velocity slip parameter. The flow rate slowed down due to the velocity slip parameter, as seen in Fig. 10(a). This occurrence occurs as a result of the slide increasing the frictional resistance between the flow and the surface. Despite this, the AA7075-EO nanofluid has a higher velocity than the Ti-6Al-4V-EO nanofluid due to the nanofluid's inclusion of metal particles (Ti) that are tightly bound. Fig. 10(b) shows a three-dimensional variation in the velocity profile, demonstrating the effect of velocity slip. Raising the velocity slip causes an even reduction in flow speed.

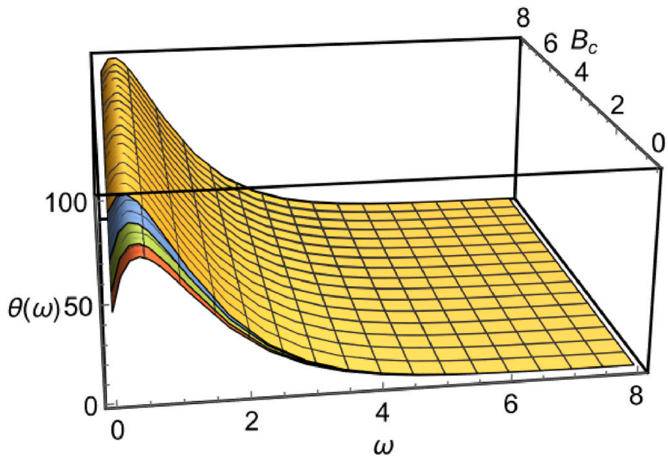

Fig. 12(b). Temperature variation versus $B_ς$. 7.2.3 Impact of radiation parameter ($\boldsymbol{N_r}$).

7.1.6. *The influence of volume fraction nanoparticle parameter (ϕ)*

In Fig. 11(a), the temperature of the system increases as a function of ϕ. It's important to note that heat transmission is influenced by fluid velocity. Heat builds up in the system when the fluid's particles are unable to move quickly enough—the temperature in the system upsurges twofold as a result. To see in-depth the system, a 3D graph has been constructed in Fig. 11(b) to illustrate the temperature behaviour in the flow. It is eye-catching that big gaps or significant changes occur when the volume fraction nanoparticle is amplified. It means that the volume fraction nanoparticle can be influenced and control the temperature behaviour throughout the system.

The Biot Number is the ratio of thermal impedance to thermal dispersion barrier in a solid mass. The impedance amid an object and its environment indicates the behaviour of the temperature changes as it spreads outward from a particular object's centre to its surroundings. As can be observed in Fig. 12(a), the Biot number has an impact on the flow's temperature. The temperature diminished as the Biot population grew, according to the graphic. Thermal resistances in the flow were magnified, leading to a rise in the flow temperature. Still, with the nanofluid characteristics properties, the temperature quickly reduced, as illustrated by this dramatic pattern. Because Ti-6Al-4V is a more extraordinary heat conductor than AA7075, AA7075-EO's temperature profile is higher than Ti-6Al-4V - EO 's. Fig. 12(b) shows a 3D graph of the flow's temperature behaviour to understand the system as a whole better. When the Biot number is enlarged, it is seen that there are significant gaps or considerable shifts. To put it another way, the Biot number is capable of influencing and controlling the system's temperature behaviour.

An example of the heat exchange between flow and surroundings affects radiation is seen in Fig. 13(a). According to the graphic, the ambient temperature affected the flow temperature. These approaches are a result of the flow and surroundings trying to achieve thermal equilibrium. Atmospheric pressure exceeds that of flowing fluid. As a result, as can be shown in Fig. 13(b), the flow temperature rises. Because of its lower temperature profile, AA7075-EO is a superior heat conductor over Ti-6Al-4V-EO. To better comprehend the system as a whole, Fig. 12 (b) displays a 3D graph of the temperature behaviour in the flow. A look at the radiation parameter reveals enormous gaps or significant

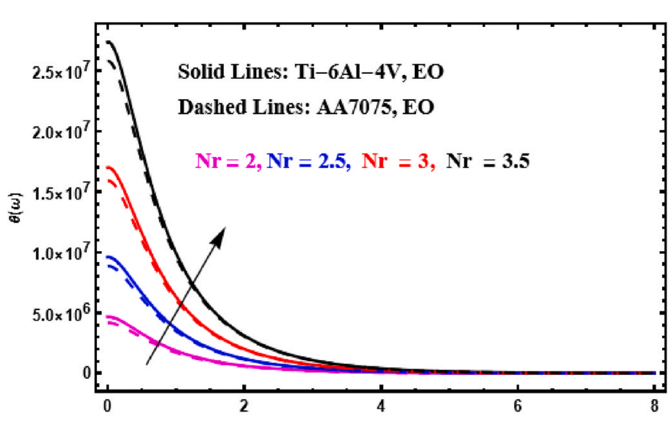

Fig. 13(a). Temperature variation versus N_r.

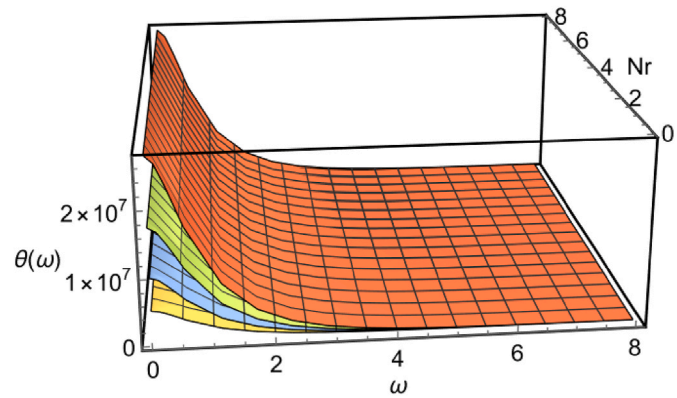

Fig. 13(b). Temperature variation versus N_r. 7.3 Local Nusselt Number.

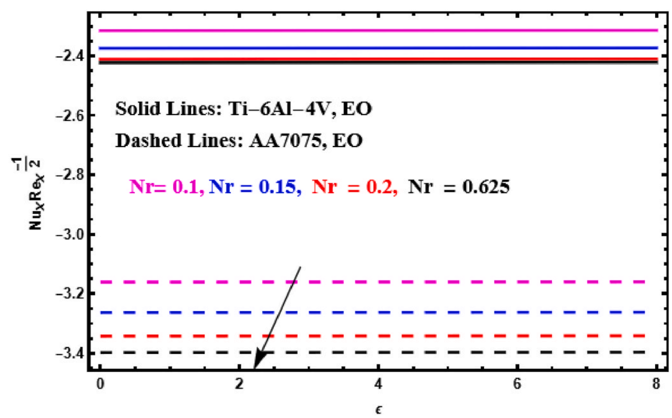

Fig. 14(a). Nusselt number Nu_x against the parameter ε.

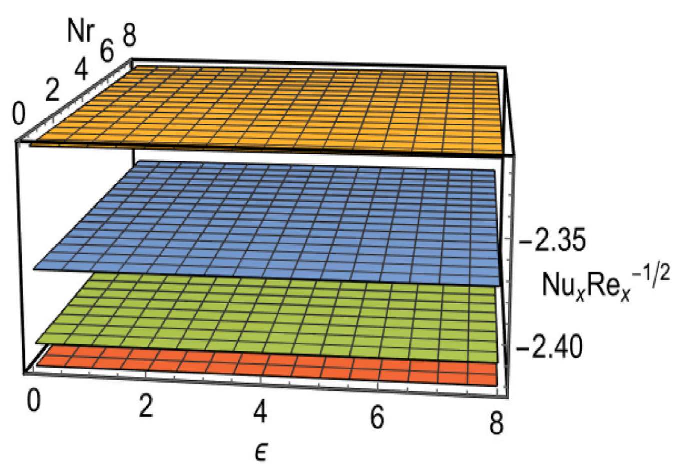

Fig. 14(b). Nusselt number Nu_x against the parameter ε.

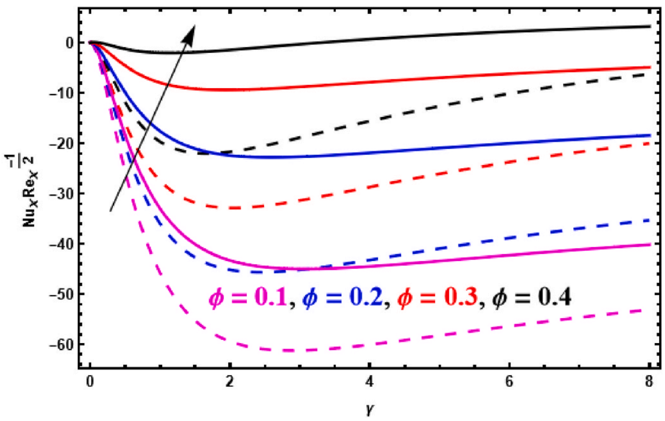

Fig. 15(a). Nusselt Number Nu_x against the parameter ϕ.

movements. For example, the radiation parameter significantly impacts the system's temperature dynamics.

7.1.7. *Impact of variable thermal conductivity (ε)*

A substance's thermal conductivity is a measure of its ability to transfer heat. Heat movement is slower in little thermal conductivity materials than in high thermal conductivity components. Fig. 14(a) showed that the changing thermal conductivity parameter negatively influenced Local Nusselt number profiles. The greater the thermal conductivity, the warmer the temperature for both nanofluids, resulting in a reduced heat transfer rate. This peculiarity explains why the heat transfer rate of both nanofluids is slower. However, because AA7075-EO is a superior heat conductor to Ti-6Al-4V -EO, it still outranks Ti-6Al-4V -EO in temperature. Fig. 14(b) is a three-dimensional graph depicting the flow's heat transmission changes over time. Significant gaps or large fluctuations can be seen in the system. As an illustration, the thermal conductivity parameter strongly influences system heat transfer dynamics.

7.1.8. *Impact of volume fraction nanoparticles parameter (ϕ)*

Because of their small size, molecules can move freely, resulting in micro convection, which can impact heat transfer. Still, the volume fraction of nanoparticles minimizes this. Both nanofluids had increased heat transfer, with Ti-6Al-4V-EO having a more excellent transmission than AA7075-EO, as illustrated in Fig. 15(a). Due to the superior thermal conductivity of Ti-6Al-4V -EO over AA7075-EO. The three-dimensional graph in Fig. 15(b) shows that the flow's heat spread changes with time. The system exhibits huge voids or variations. For example, the volume fraction nanoparticle parameter has a substantial influence on the system heat transport dynamics.

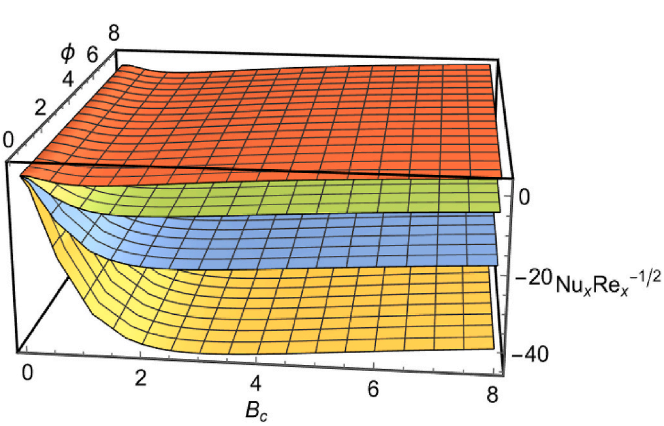

Fig. 15(b). Nusselt Number Nu_x against the parameter ϕ.

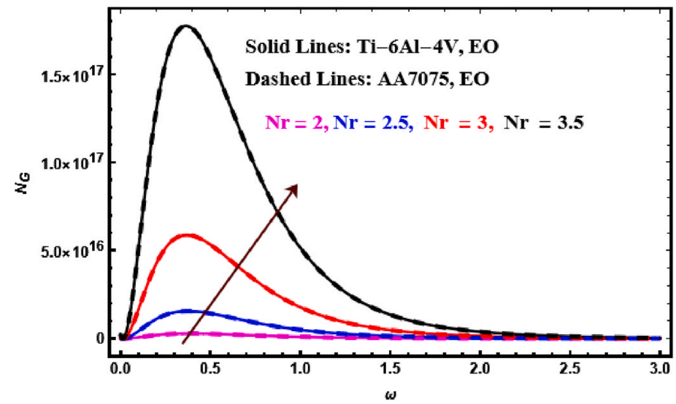

Fig. 16(a). Entropy variation against N_r.

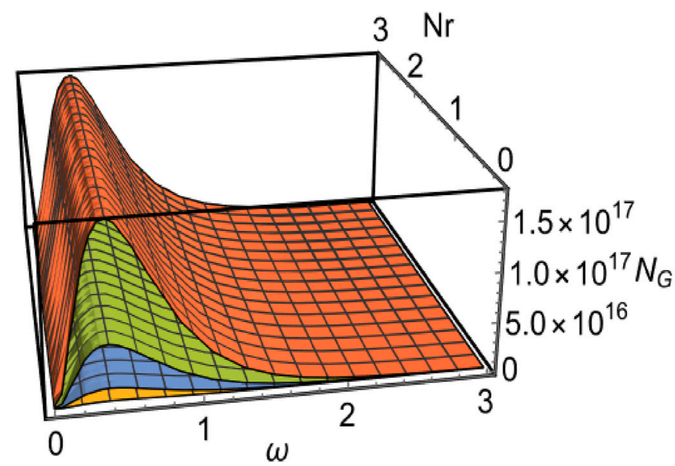

Fig. 16(b). Entropy variation against N_r. 7.4.2 Impact of Reynolds number (R_e).

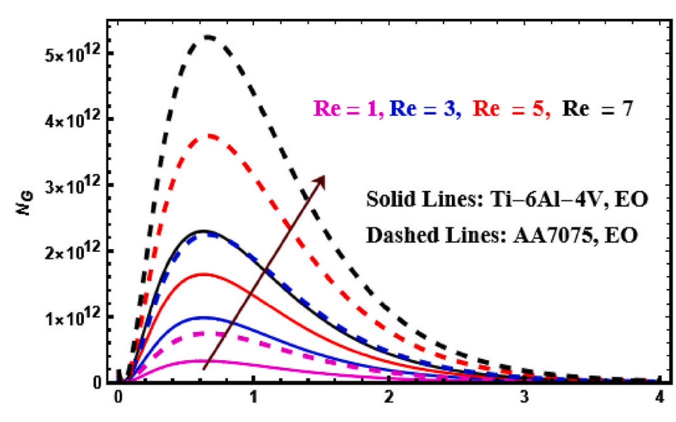

Fig. 17(a). Entropy variation versus R_e.

7.2. *Entropy profiles*

7.2.1. *Impact of radiation parameter (N_r)*

The flow's radiation response can produce a heat exchange between the flow and its environment. Entropy may be shown in Fig. 16(a) as a result of this factor. The paper's main point was that the energy in the system is irrevocably altered. The augmented entropy value of Ti-6Al-4V -EO nanofluid compared to AA7075-EO is significant. AA7075 has a weaker bond with based fluid than does Ti-6Al-4V. Entropy, in due

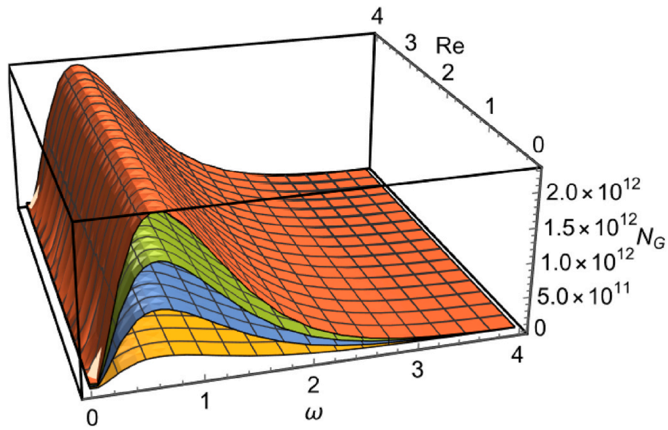

Fig. 17(b). Entropy variation versus R_e. 7.5 Overall Heat Transfer Rate for Ti-6Al-4V/EO and AA7075/EO.

Table 4

Calculation of Nusselt number $Nu_x Re_x^{\frac{-1}{2}}$ for $Pr = 6450$.

Nr	Pr	ϕ	$\in$	B_c	Nu_x (Ti-6Al-4V/EO)	Nu_x (AA7075/EO)
0.1	6450	0.1	0.1	0.1	−1.701614	−2.424476
0.15					−1.774210	−2.533901
0.2					−1.827336	−2.624491
0.25					−1.858609	−2.693901
		0.1			−1.701614	−2.424476
		0.2			−0.867089	−1.924473
		0.3			−0.326379	−1.475551
		0.4			0.034186	−1.046773
			0.1		−1.701614	−2.424476
			0.2		−1.701605	−2.424466
			0.3		−1.701597	−2.424455
			0.4		−1.701588	−2.424445
				0.1	−1.701614	−2.424476
				0.15	−3.442115	−4.871366
				0.2	−5.473276	−7.717921
				0.25	−7.656352	−10.770367

course, is incompetent to threaten the arrangement immediately. Fig. 16 (b) shows how the flow's entropy evolves on a three-dimensional graph. The system is riddled with holes or inconsistencies. As an example, the radiation parameter has a considerable effect on system heat transport dynamics.

According to Fig. 17(a), inertia causes the entropy of a system to intensify by way of the Reynold number rises. As a result, the nanofluid particles travel faster and display a more significant number of Reynold-number abnormalities. The development of the large difference entropy of Ti-6Al-4V -EO nanofluid with AA7075-EO it's astonishing. For example, Ti-6Al-4V has a far larger propensity for based fluids than AA7075. As nothing more than a result, entropy cannot cause the system to disintegrate rapidly. For example, a three-dimensional graph of the flow's entropy is depicted in Fig. 17(b). There are several flaws in the arrangement. For instance, the Reynolds number significantly impacts the dynamics of the system's entropy.

Thermal conductivity is improved in nanofluids due to the superiority of AA7075's thermal conductivity compared to Ti-6Al-4V. To aid the reader, the findings are shown in Table 4. The negative values of heat transmission reveal that the heat was transferred from the flow towards the surface.

Heat transfer rates can be improved by aggregate radiation, as shown in Table 3. Since electromagnetic waves are emitted from a source and received at a receiver, radiation is well-known as the quickest means of transmitting heat. Instead of AA7075-EO, the Ti-6Al-4V -EO is found to have the radiation essence. This way, radiation is conceivably engaged as a catalyst to increase heat transmission for Ti-6Al-4V -EO.

Because of their small size, molecules can move freely, resulting in micro convection, which can impact heat transfer. Still, the volume fraction of nanoparticles minimizes this. Both nanofluids degraded the heat transfer, but AA7075-EO has a more extraordinary transmission than Ti-6Al-4V -EO. Because AA7075-EO is a better heat sink than Ti-6Al-4V -EO.

It is detected that the variable thermal conducting almost does not affect the heat transmission in the system. The reduction is way too small to have an impact on the flow. On the other hand, the Biot number increased in both nanofluids, although AA7075-EO had a higher heat transmission than Ti-6Al-4V -EO. It's because AA7075-EO is a better heat conductor than Ti-6Al-4V -EO.

8. Conclusion

In the present research, a theoretical investigation, the thermal and entropy properties of 3-GNF are being investigated. A numerical solution to governing differential formulas may be obtained using the homotopy analysis approach. Without a doubt, the results have been subjected to extensive investigation and discussion by all the parties involved. Considering the findings of the research, the following deductions may be illustrated.

- To increase the flow velocity, it is possible to increase the number of third-grade parameters and the Reynolds number.
- The presence of radiation parameters is the only factor that causes temperature profiles to build up in the system.
- In the meantime, the volume fraction of nanoparticles parameter and the Biot number contribute to the cooling down of the system.
- Porous media, fractional size of nanoparticles, suction, and velocity slip parameters are the other factors that will cause the flow's velocity to decelerate.
- As widely discussed, the volume fraction of nanoparticles, radiation parameters, and Biot number can boost heat transportation, but variable thermal conductivity occurs to be reducing the transmission.
- The entropy of the system will be amplified as the radiation, and the Reynolds number will be augmented.
- Overall, based on the findings, AA7075-EO possesses better characteristics and properties in enhancing the physical quantities in the systems than Ti-6Al-4V -EO.

CRediT authorship contribution statement

Syed M. Hussain: Methodology. **Misbah Arshad:** Writing – original draft. **Hijaz Ahmad:** Investigation. **Wasim Jamshed:** Software. **Kamel Guedri:** Validation. **Muhammad Amer Qureshi:** Visualization. **Siti Suzilliana Putri Mohamed Isa:** Supervision, Data curation. **Abdulrazak H. Almaliki:** Methodology, Data curation. **Mustafa Bayram:** Software, Conceptualization.

Funding

This research work was funded by Umm Al-Qura University, Saudi Arabia under grant number: 25UQU4331317GSSR04.

Conflict of interest

None.

Acknowledgement

The authors extend their appreciation to Umm Al-Qura University, Saudi Arabia for funding this research work through grant number: 25UQU4331317GSSR04.

References

Abraham, J. P., & Sparrow, E. M. (2005). Friction drag resulting from the simultaneous imposed motions of a freestream and its bounding surface. *International Journal of Heat and Fluid Flow, 26*(2), 289–295.

Abu-Hamdeh, N. H., Aljinaidi, A. A., Eltaher, M. A., Almitani, K. H., Alnefaie, K. A., Abusorrah, A. M., & Safaei, M. R. (2021). Implicit Finite Difference Simulation of Prandtl-Eyring Nanofluid over a Flat Plate with Variable Thermal Conductivity: A Tiwari and Das Model. *Mathematics, 9*(24), 3153.

Adesanya, S. O., & Makinde, O. D. (2015). Thermodynamic analysis for a third grade fluid through a vertical channel with internal heat generation. *Journal of Hydrodynamics, 27*(2), 264–272.

Adnan, N., Khan, S. I. U., Khan, U., Ahmed, N., Mohyud-Din, S. T., Khan, I., & Nisar, K. S. (2021). Thermal transport investigation in AA7072 and AA7075 aluminum alloys nanomaterials based radiative nanofluids by considering the multiple physical flow conditions. *Scientific Reports, 11*(1), 9837.

Aïboud, S., & Saouli, S. (2010). Entropy analysis for viscoelastic magnetohydrodynamic flow over a stretching surface. *International Journal of Non-Linear Mechanics, 45*(5), 482–489.

Akinshilo, A. T., & Sobamowo, G. M. (2017). Perturbation solutions for the study of MHD blood as a third grade nanofluid transporting gold nanoparticles through a porous channel. *J. Appl. Comput. Mech., 3*(2), 103–113.

Ali, K., Faridi, A. A., Ahmad, S., Jamshed, W., Khan, N., & Alam, M. M. (2022). Quasi-linearization analysis for heat and mass transfer of magnetically driven 3rd-grade (Cu-TiO2/engine oil) nanofluid via a convectively heated surface. *International Communications in Heat and Mass Transfer, 135*, Article 106060.

Alkathiri, A. A., Jamshed, W., Eid, M. R., & Bouazizi, M. L. (2022). Galerkin finite element inspection of thermal distribution of renewable solar energy in presence of binary nanofluid in parabolic trough solar collector. *Alexandria Engineering Journal, 61*(12), 11063–11076. others.

Alzahrani, E. O., Shah, Z., Dawar, A., & Malebary, S. J. (2019). Hydromagnetic mixed convective third grade nanomaterial containing gyrotactic microorganisms toward a horizontal stretched surface. *Alexandria Engineering Journal, 58*(4), 1421–1429.

Anantha Kumar, K., Sugunamma, V., & Sandeep, N. (2020). Effect of thermal radiation on MHD Casson fluid flow over an exponentially stretching curved sheet. *Journal of Thermal Analysis and Calorimetry, 140*, 2377–2385.

Andersson, H., Bech, K., & Dandapat, B. (1992). Magnetohydrodynamic flow of a power-law fluid over a stretching sheet. *International Journal of Non-Linear Mechanics, 27*(6), 929–936.

Baris, S. (2003). Steady three-dimensional flow of a second grade fluid towards a stagnation point at a moving flat plate. *Turkish Journal of Engineering and Environmental Sciences, 27*(1).

Benetti, M., Aloisi, G., Reverdin, G., Risi, C., & Sèze, G. (2015). Importance of boundary layer mixing for the isotopic composition of surface vapor over the subtropical North Atlantic Ocean. *J. Geophys. Res. Atmospheres, 120*(6), 2190–2209.

Crane, L. J. (1970). Flow past a stretching plate. *Z. Für Angew. Math. Phys. ZAMP, 21*, 645–647.

Davey, A. (1961). Boundary-layer flow at a saddle point of attachment. *Journal of Fluid Mechanics, 10*(4), 593–610.

Ellahi, R., & Riaz, A. (2010). Analytical solutions for MHD flow in a third-grade fluid with variable viscosity. *Mathematical and Computer Modelling, 52*(9–10), 1783–1793.

Epifanov, V. (2011). Boundary layer. In *Thermopedia*. Begel House Inc.

Fosdick, R., & Rajagopal, K. (1980). Thermodynamics and stability of fluids of third grade. *Proc. R. Soc. Lond. Math. Phys. Sci., 369*(1738), 351–377.

Gaffar, S. A., Prasad, V. R., Bég, O. A., Khan, M. H. H., & Venkatadri, K. (2018). Radiative and magnetohydrodynamics flow of third-grade viscoelastic fluid past an isothermal inverted cone in the presence of heat generation/absorption. *Journal of the Brazilian Society of Mechanical Sciences and Engineering, 40*(3), 127.

Hayat, T., Naz, R., Asghar, S., & Mesloub, S. (2012). Soret–Dufour effects on three-dimensional flow of third grade fluid. *Nuclear Engineering and Design, 243*, 1–14.

Hayat, T., Nazar, H., Imtiaz, M., Alsaedi, A., & Ayub, M. (2017). Axisymmetric squeezing flow of third grade fluid in presence of convective conditions. *Chinese Journal of Physics, 55*(3), 738–754.

Hussnain, S., Mehmood, A., & Ali, A. (2012). Three-dimensional channel flow of second grade fluid in rotating frame. *Applied Mathematics and Mechanics, 33*, 289–302.

Iqbal, Z., Azhar, E., & Maraj, E. (2021). Performance of nano-powders SiO2 and SiC in the flow of engine oil over a rotating disk influenced by thermal jump conditions. *Phys. Stat. Mech. Its Appl., 565*, Article 125570.

Jamshed, W., & Aziz, A. (2018). A comparative entropy based analysis of Cu and Fe3O4/methanol Powell-Eyring nanofluid in solar thermal collectors subjected to thermal radiation, variable thermal conductivity and impact of different nanoparticles shape. *Results Physics, 9*, 195–205.

Jamshed, W., Nisar, K. S., Ibrahim, R. W., Shahzad, F., & Eid, M. R. (2021). Thermal expansion optimization in solar aircraft using tangent hyperbolic hybrid nanofluid: A solar thermal application. *Journal of Materials Research and Technology, 14*, 985–1006.

Jawad, M., Khalifa, H. A. E.-W., Shaaban, A. A., Akgül, A., Riaz, M. B., & Sadiq, N. (2024). Characteristics of heat transportation in MHD flow of chemical reactive micropolar nanofluid with moving slip conditions across stagnation points. *Results Eng, 21*, Article 101954.

Jawad, M., Sadiq, N., & Ali, M. R. (2024). Analysis of chemical reactive tangent hyperbolic nanofluid flow with joule heating and motile microorganisms through stretchable surface. *BioNanoScience, 14*(2), 605–618.

Lakshmisha, K. N., Venkateswaran, S., & Nath, G. (1988). *Three-dimensional unsteady flow with heat and mass transfer over a continuous stretching surface*.

Liao, S.-J. (1992). *The proposed homotopy analysis technique for the solution of nonlinear problems*. Shanghai: Shanghai Jiao Tong University. PhD Thesis, Ph. D. Thesis.

Liao, S.-J. (1999a). *An explicit totally analytic approximation of Blasius viscous flow problems*.

Liao, S.-J. (1999b). A simple approach of enlarging convergence regions of perturbation approximations. *Nonlinear Dynamics, 19*, 93–111.

Liao, S. (2004). On the homotopy analysis method for nonlinear problems. *Applied Mathematics and Computation, 147*(2), 499–513.

Liao, S.-J., & Cheung, K. F. (2003). Homotopy analysis of nonlinear progressive waves in deep water. *Journal of Engineering Mathematics, 45*, 105–116.

Loganathan, K., Mohana, K., Mohanraj, M., Sakthivel, P., & Rajan, S. (2021). Impact of third-grade nanofluid flow across a convective surface in the presence of inclined lorentz force: An approach to entropy optimization. *Journal of Thermal Analysis and Calorimetry, 144*(5), 1935–1947.

Loganathan, K., & Rajan, S. (2020). An entropy approach of Williamson nanofluid flow with Joule heating and zero nanoparticle mass flux. *Journal of Thermal Analysis and Calorimetry, 141*(6), 2599–2612.

Magyari, E., & Keller, B. (2000). Exact solutions for self-similar boundary-layer flows induced by permeable stretching walls. *Eur. J. Mech.-BFluids, 19*(1), 109–122.

Mahanthesh, B., & Joseph, T. (2019). Dynamics of magneto-nano third-grade fluid with Brownian motion and thermophoresis effects in the pressure type die. *J. Nanofluids, 8*(4), 870–875.

Makinde, O. D. (2011). Second law analysis for variable viscosity hydromagnetic boundary layer flow with thermal radiation and Newtonian heating. *Entropy, 13*(8), 1446–1464.

Makinde, O. D., & Aziz, A. (2011). Boundary layer flow of a nanofluid past a stretching sheet with a convective boundary condition. *International Journal of Thermal Sciences, 50*(7), 1326–1332.

Makinde, O. D., Mahanthesh, B., Gireesha, B. J., Shashikumar, N., Monaledi, R., & Tshehla, M. (2018). MHD nanofluid flow past a rotating disk with thermal radiation in the presence of aluminum and titanium alloy nanoparticles. In *Defect and diffusion forum* (pp. 69–79). Trans Tech Publ.

McKee, K. I. (2024). Magnetohydrodynamic flow control in Hele-Shaw cells. *Journal of Fluid Mechanics, 993*, A11.

Mustafa, M., Nawaz, M., Hayat, T., & Alsaedi, A. (2014). MHD boundary layer flow of second-grade nanofluid over a stretching sheet with convective boundary conditions. *J. Aerosp. Eng., 27*(4), Article 04014006.

Naz, R., Tariq, S., Sohail, M., & Shah, Z. (2020). Investigation of entropy generation in stratified MHD Carreau nanofluid with gyrotactic microorganisms under Von Neumann similarity transformations. *Eur. Phys. J. Plus, 135*(2), 178.

Polidori, G., Fohanno, S., & Nguyen, C. (2007). A note on heat transfer modelling of Newtonian nanofluids in laminar free convection. *International Journal of Thermal Sciences, 46*(8), 739–744.

Pozhar, L. A. (2000). Structure and dynamics of nanofluids: Theory and simulations to calculate viscosity. *Physical Review E - Statistical Physics, Plasmas, Fluids, and Related Interdisciplinary Topics, 61*(2), 1432.

Rafati, M., Hamidi, A., & Niaser, M. S. (2012). Application of nanofluids in computer cooling systems (heat transfer performance of nanofluids). *Applied Thermal Engineering, 45*, 9–14.

Ramasekhar, G., et al. (2024). Heat transfer innovation of engine oil conveying SWCNTs-MWCNTs-TiO2 nanoparticles embedded in a porous stretching cylinder. *Scientific Reports, 14*(1), Article 16448.

Ramasekhar, G., & Jawad, M. (2024). Characteristics of MWCNT, SWCNT, Cu and water based on magnetized flow of nanofluid with Soret and Dufour effects induced by moving wedge: Consequence of Falkner–Skan power law. *Numer. Heat Transf. Part Appl*, 1–15.

Ramzan, M., Bilal, M., Farooq, U., & Chung, J. D. (2016). Mixed convective radiative flow of second grade nanofluid with convective boundary conditions: An optimal solution. *Results Physics, 6*, 796–804.

Rashidi, M. M., Shahmohamadi, H., & Dinarvand, S. (2008). Analytic approximate solutions for unsteady two-dimensional and axisymmetric squeezing flows between parallel plates. *Mathematical Problems in Engineering, 2008*(1), Article 935095.

Reddy, G. J., Hiremath, A., & Kumar, M. (2018). Computational modeling of unsteady third-grade fluid flow over a vertical cylinder: A study of heat transfer visualization. *Results Physics, 8*, 671–682.

Rivlin, R. S., & Ericksen, J. L. (1997). Stress-deformation relations for isotropic materials. *Collect. Pap. RS Rivlin, II*, 911–1013.

Sajid, M., Mahmood, R., & Hayat, T. (2008). Finite element solution for flow of a third grade fluid past a horizontal porous plate with partial slip. *Comput. Math. Appl., 56*(5), 1236–1244.

Sajid, M., Mughees, M., Ali, N., & Shahzad, H. (2019). A theoretical analysis of blade coating for third-grade fluid. *Journal of Plastic Film & Sheeting, 35*(3), 218–238.

Schlichting, H., & Gersten, K. (2016). *Boundary-layer theory*. springer.

Shah, Z., Babazadeh, H., Kumam, P., Shafee, A., & ounthong, P. (2019). Numerical simulation of magnetohydrodynamic nanofluids under the influence of shape factor and thermal transport in a porous media using CVFEM. *Front. Phys., 7*(11), 1–10.

Shah, Z., Kumam, P., Dawar, A., Alzahrani, E. O., & Thounthong, P. (2019). Study of the couple stress convective micropolar fluid flow in a hall MHD generator system. *Front. Phys., 7*, 171.

Shahzad, F., Jamshed, W., Ibrahim, R. W., Nisar, K. S., Qureshi, M. A., Hussain, S. M., … Yahia, I. S. (2021). Comparative Numerical Study of Thermal Features Analysis between Oldroyd-B Copper and Molybdenum Disulfide Nanoparticles in Engine-Oil-Based Nanofluids Flow. *Coatings, 11*(10), 1196.

Shehzad, S., Abbasi, F., Hayat, T., & Ahmad, B. (2016). Cattaneo-Christov heat flux model for third-grade fluid flow towards exponentially stretching sheet. *Applied Mathematics and Mechanics, 37*, 761–768.

Shehzad, S., Hussain, T., Hayat, T., Ramzan, M., & Alsaedi, A. (2015). Boundary layer flow of third grade nanofluid with Newtonian heating and viscous dissipation. *J. Cent. South Univ., 22*, 360–367.

Shoaib, M., Siddiqui, A., Rana, M., & Imran, A. (2016). Three-dimensional flow of a second grade fluid along an infinite horizontal plane wall with periodic suction. *Res. J. Eng. Technol. Sci. ASRJETS, 18*(1), 153–170.

Sohail, M., Abodayeh, K., & Nazir, U. (2024). Implementation of finite element scheme to study thermal and mass transportation in water-based nanofluid model under quadratic thermal radiation in a disk. *Mechanics of Time-Dependent Materials, 28*(3), 1049–1072.

Sohail, M., Naz, R., Shah, Z., Kumam, P., & Thounthong, P. (2019). Exploration of temperature dependent thermophysical characteristics of yield exhibiting non-Newtonian fluid flow under gyrotactic microorganisms. *AIP Advances, 9*(12).

Sparrow, E. M., & Abraham, J. P. (2005). Universal solutions for the streamwise variation of the temperature of a moving sheet in the presence of a moving fluid. *International Journal of Heat and Mass Transfer, 48*(15), 3047–3056.

Sullerey, R., Mishra, S., & Pradeep, A. (2002). Application of boundary layer fences and vortex generators in improving performance of S-duct diffusers. *J Fluids Eng, 124*(1), 136–142.

Takhar, H. S., Chamkha, A. J., & Nath, G. (2001). Unsteady three-dimensional MHD-boundary-layer flow due to the impulsive motion of a stretching surface. *Acta Mechanica, 146*(1), 59–71.

Torres-Mendieta, R., Mondragón, R., Puerto-Belda, V., Mendoza-Yero, O., Lancis, J., Juliá, J. E., & Mínguez-Vega, G. (2016). Characterization of Tin/Ethylene glycol solar nanofluids synthesized by femtosecond laser radiation. *ChemPhysChem, 18*(9), 1055–1060.

Tulapurkara, E. (2005). Hundred years of the boundary layer—some aspects. *Sadhana, 30*, 499–512.

Turkyilmazoglu, M. (2016). Flow and heat simultaneously induced by two stretchable rotating disks. *Physics of Fluids, 28*(4).

Vleggaar, J. (1977). Laminar boundary-layer behaviour on continuous, accelerating surfaces. *Chemical Engineering Science, 32*(12), 1517–1525.

Wang, C. (1984). The three-dimensional flow due to a stretching flat surface. *Physics of Fluids, 27*(8), 1915–1917.

Waseem, M., Jawad, M., Aldalbahi, M. M., Naeem, S., Gull, H., & Majeed, A. (2025). Statistical and mathematical modeling of viscoelastic 3D Casson nanofluid flow with activation energy and motile microbes induced by exponential sheet bounding with Darcy-Forchheimer porous medium. *Multiscale Multidiscip. Model. Exp. Des., 8*(1), 14.

Yuan, S., Leng, Y., Fouly, A., Awwad, E. M., Nazir, U., & Sohail, M. (2024). A study of four-phase fluid and thermal enhancement based on tetra-hybrid nanofluid considering temperature jump on a spinning sphere. *Case Studies in Thermal Engineering, 58*, Article 104353.

Yürüsoy, M., & Pakdemirli, M. (2002). Approximate analytical solutions for the flow of a third-grade fluid in a pipe. *International Journal of Non-Linear Mechanics, 37*(2), 187–195.